High-p_T results and parton density functions from ATLAS

Javier Llorente Merino, on behalf of the ATLAS Collaboration[1,*]

[1]Simon Fraser University

Abstract. The ATLAS detector at the LHC is an ideal experiment to rigorously test QCD in a large variety of final states. This talk will focus on recent results over a wide range of energies, which are particularly sensitive to parton density functions. We will review results with high-p_T jets, photons and vector bosons. We will then discuss fits to determine parton distribution functions (PDFs) using these diverse sets of measurements from the ATLAS experiment. These measurements are used in combination with deep-inelastic scattering data from HERA. Particular attention is paid to the correlation of systematic uncertainties within and between the various ATLAS data sets and to the impact of model, theoretical and parameterisation uncertainties. Finally, we will also present results on the determination of α_s.

ATL-PHYS-PROC-2022-083
06 October 2022

1 Introduction

By virtue of the factorisation theorem [1], the differential QCD cross section for $2 \to 2$ processes in hadron-hadron collisions can be written as a convolution of the partonic cross section $\hat{\sigma}(\vec{x}, \mu_R^2)$, which is of perturbative nature and depends on the renormalisation scale μ_R, with functions parameterising the non-perturbative properties of the initial and final states, *i.e.*

$$d\sigma = \sum_{i,j,a,b} \int_\Omega d^2\vec{x} d^2\vec{z}\, f_i(x_1, \mu_F^2) f_j(x_2, \mu_F^2) \times d\hat{\sigma}_{ij\to ab}(\vec{x}, \mu_R^2) \times D_a^h(z_3, \mu_f^2) D_b^h(z_4, \mu_f^2). \quad (1)$$

The initial state is characterised by the functions $f_i(x_j, \mu_F^2)$, which parameterise the fraction of momentum x carried by partons i and j, as a function of the factorisation scale μ_F. On the other hand, the final state is characterised by the fragmentation functions, $D_a^h(z, \mu_f^2)$, parameterising the fraction of momentum z carried by a hadron h when fragmented out of a final-state parton a as a function of the fragmentation scale μ_f.

The ATLAS detector provides a unique environment for testing each of the components of Equation 1. This is achieved through the interpretation of different measurements, sensitive to each of the aspects mentioned above, by means of the comparison of the experimental data to different models.

*e-mail: javier.llorente.merino@cern.ch

2 The initial state: parton distribution functions

A determination of the parton distribution functions has been recently published by the ATLAS Collaboration in Ref. [2]. This determination makes use of a combination of deep inelastic scattering data from HERA [3], together with various ATLAS measurements at different values of the centre-of-mass energy: $\sqrt{s}$ = 7, 8 and 13 TeV. This includes the production of W and Z bosons as well as photons, both inclusively and in association with jets. Measurements of inclusive jets and $t\bar{t}$ production are also considered. Table 1 summarises the input datasets used in the fit.

Data set	$\sqrt{s}$ [TeV]	Luminosity [fb^{-1}]	Decay channel	Observables entering the fit
Inclusive $W, Z/\gamma^*$	7	4.6	e, μ combined	η_ℓ (W), y_Z (Z)
Inclusive Z/γ^*	8	20.2	e, μ combined	$\cos\theta^*$ in bins of $y_{\ell\ell}$, $m_{\ell\ell}$
Inclusive W	8	20.2	μ	η_μ
$W^\pm$ + jets	8	20.2	e	p_{T}^W
Z + jets	8	20.2	e	$p_{\mathrm{T}}^{\mathrm{jet}}$ in bins of $\lvert y^{\mathrm{jet}}\rvert$
$t\bar{t}$	8	20.2	lepton + jets, dilepton	$m_{t\bar{t}}$, p_{T}^t, $y_{t\bar{t}}$
$t\bar{t}$	13	36	lepton + jets	$m_{t\bar{t}}$, p_{T}^t, y_t, $y_{t\bar{t}}^{\mathrm{b}}$
Inclusive isolated γ	8, 13	20.2, 3.2	-	E_{T}^γ in bins of η^γ
Inclusive jets	7, 8, 13	4.5, 20.2, 3.2	-	$p_{\mathrm{T}}^{\mathrm{jet}}$ in bins of $\lvert y^{\mathrm{jet}}\rvert$

Table 1. The ATLAS data sets used for the PDF determination, together with the HERA DIS data [2].

The measurements are compared to NNLO QCD + NLO EW predictions, which are then fitted to the data. The fit consists in the minimisation of a χ^2 function in a 21-dimensional parameter space, which fully takes into account the correlations between the measurements and their uncertainties. The results of the fit are compared to global PDF sets such as CT18 [4], NNPDF 3.1 [5] and MSHT20 [6].

Figure 1 shows the determined parton distribution functions for the valence d-quark as well as for gluons at a scale Q^2 = 1.9 GeV^2, together with the results from other global PDF fits, including CT18 and CT18A [4] as well as HERAPDF [3].

3 The hard scattering: fixed-order matrix elements

ATLAS has recently published several measurements sensitive to the calculation of the fixed-order matrix element in Equation 1. The data are compared to theoretical predictions at different orders of the perturbative expansion, up to NNLO pQCD.

Reference [7] presents a measurement of the Z+jets cross section with high-p_T jets in different angular configurations between the Z boson and the leading jet. The results are compared to NNLO QCD + NLO EW theoretical predictions and include a comparison of the ratio of the p_T of the Z boson to the p_T of the closest jet in collinear and back-to-back topologies. The left part of Figure 2 shows the Z+jets cross section as a function of the angular distance $\Delta R = \sqrt{(\Delta y)^2 + (\Delta\varphi)^2}$, being y the rapidity and φ the azimuthal coordinate, between the Z boson and the closest jet. The measurements are compared to different versions of MadGraph5_aMC@NLO [8] and Sherpa [9] with different parton shower matching schemes. Sherpa 2.2.11 and MG5_aMC@NLO with NLO matrix elements and FxFx matching [10] provide the best description of the data.

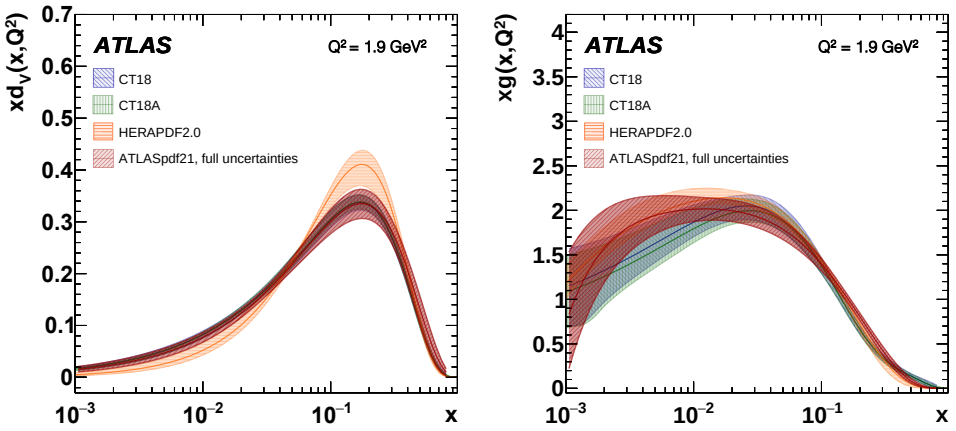

Figure 1. The valence d-quark parton density, $x \cdot d_v(x, Q^2)$ (left) and gluon parton density, $x \cdot g(x, Q^2)$ (right) at $Q^2 = 1.9$ GeV^2, as determined from the ATLAS analysis [2].

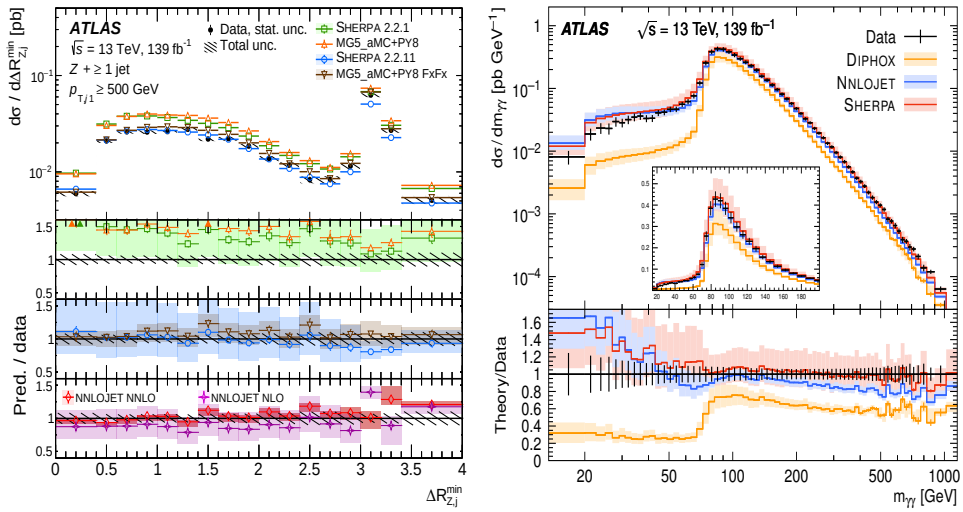

Figure 2. The Z+jets cross section as a function of the ΔR distance between the Z boson and the closest jet (left, [7]). The diphoton cross section as a function of the invariant mass of the two photons (right, [12]).

The diphoton cross section is presented by ATLAS in Ref. [12]. Measurements are shown as a function of different kinematic variables including, among others, the invariant mass and the transverse momentum of the diphoton system, as well as the angular separation between the two photons. The results are compared to theoretical predictions up to NNLO. The production cross section for pairs of photons as a function of the invariant mass of the diphoton pair is shown on the right-hand side of Figure 2. While the fixed-order NLO

predictions by DiPhox [13] fail to model the shape of the distributions and underestimate the total cross section, the NNLO predictions show a large improvement with respect to the previous order. The resummed predictions from Sherpa [9] agree well with the data in all regions of the phase space.

A measurement of Transverse Energy-Energy Correlations, i.e. the energy weighted distributions of the differences in azimuth between pairs of jets, and their azimuthal asymmetry, is presented in Ref. [11]. The results are compared to theoretical predictions up to NLO, corrected for non-perturbative effects, and the value of the strong coupling constant at the Z mass pole, $\alpha_s(m_Z)$, is determined. A study of the running of $\alpha_s(Q)$, obtained from fits in different kinematic regions, is also presented. Figure 3 shows the values of $\alpha_s(Q)$ together with the NLO solution to the Renormalisation Group Equation. The value of the strong coupling constant at the Z mass pole, obtained from a global fit to the TEEC distributions in different kinematic regimes, is

$$\alpha_s(m_Z) = 0.1196 \pm 0.0001\ (\text{stat.}) \pm 0.0004\ (\text{sys.})^{+0.0071}_{-0.0104}\ (\text{scale}) \pm 0.0011\ (\text{PDF}) \pm 0.0002\ (\text{NP}),$$

where experimental uncertainties (statistical and systematic sources) and theoretical uncertainties (due to the choice of the QCD scales, PDFs and non-perturbative corrections) are included.

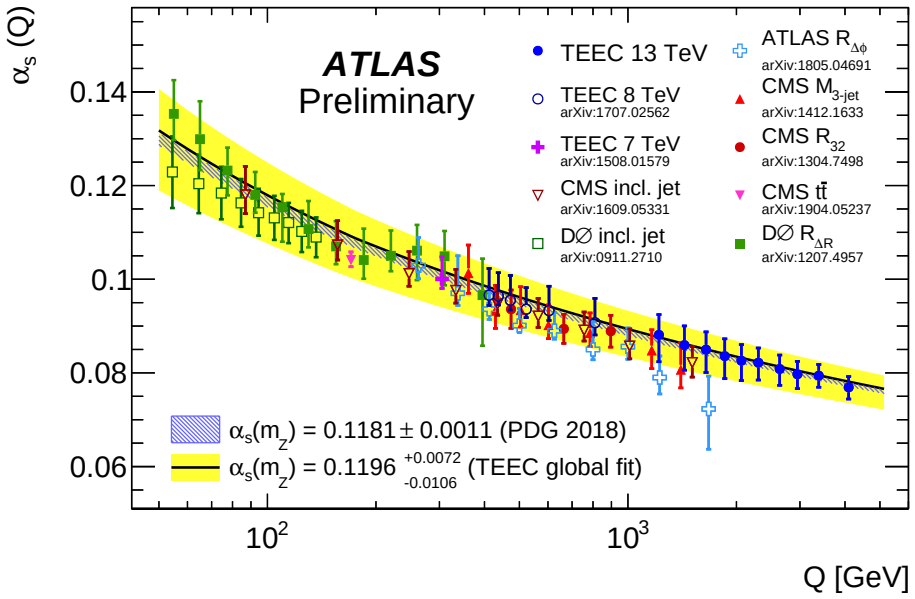

Figure 3. Comparison of the values of $\alpha_s(Q)$ determined from fits to the TEEC functions with the QCD prediction using the world average as input (blue band) and the value obtained from the global fit (yellow band). Results from previous analyses, both from ATLAS and from other experiments, are also included, showing an excellent agreement with the current measurements and with the world average.

4 The final state: heavy quark fragmentation functions

The fragmentation of heavy quarks into hadrons is explored by the ATLAS Collaboration in Refs. [14, 15]. Reference [14] presents a measurement of the fragmentation properties of charged B mesons, decaying through $B^{\pm} \rightarrow J/\psi K^{\pm}$, inside jets. More specifically, the

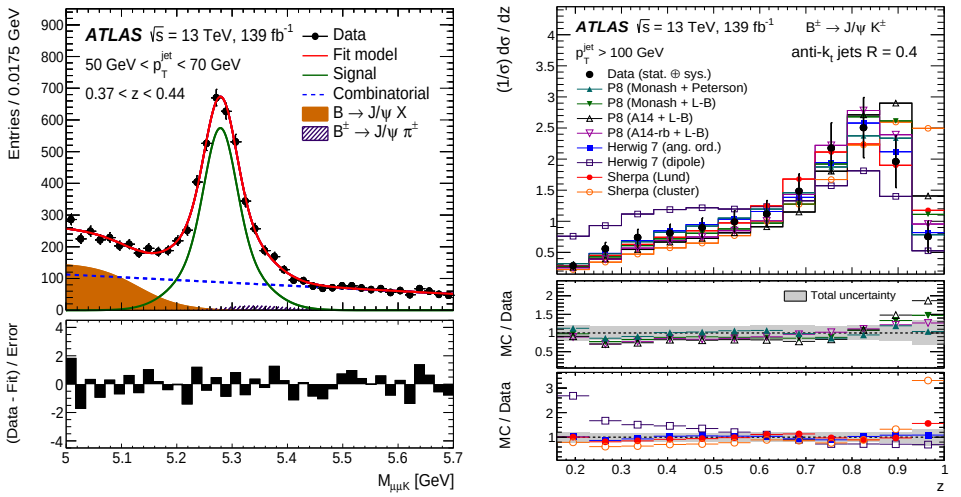

Figure 4. The invariant mass of the $B^{\pm}$ candidates reconstructed in a particular bin of jet p_T and z (left). The longitudinal profile distribution for jets with $p_T > 100$ GeV (right) [14]

longitudinal and transverse profiles of the momentum of $B^{\pm}$ mesons, $\vec{p}_B$, with respect to the momentum of the jets containing them, $\vec{p}_J$, defined as

$$z = \frac{\vec{p}_J \cdot \vec{p}_B}{\left|\vec{p}_J\right|^2}; \qquad p_T^{\mathrm{rel}} = \frac{\left|\vec{p}_J \times \vec{p}_B\right|}{\left|\vec{p}_J\right|}, \tag{2}$$

are measured. The results show a significant dependence of the studied variables on the modelling of gluon splittings $g \rightarrow b\bar{b}$, and an important spread of the different Monte Carlo predictions with respect to the data. Figure 4 shows the invariant mass of the reconstructed $B^{\pm}$ candidates, as well as the longitudinal profile for jets with $p_T > 100$ GeV.

Reference [15] presents a measurement of observables sensitive to the fragmentation functions of b-quarks in dileptonic $t\bar{t}$ events containing an electron and a muon. The measurement is performed using jets containing a displaced secondary vertex with at least four tracks originating from it, which are used to reconstruct the charged momentum of the B-hadron, $\vec{p}_b^{\,\mathrm{ch}}$. The charged momentum of the jet, $\vec{p}_{\mathrm{jet}}^{\,\mathrm{ch}}$, is reconstructed using all tracks geometrically associated to it.

The measured distributions, including the charged longitudinal profile as well as the number of charged particles originating from the B-hadron decay, are shown in Figure 5. The distributions are compared to different Monte Carlo expectations with the $t\bar{t}$ matrix elements calculated up to NLO, providing a generally reasonable agreement with the data.

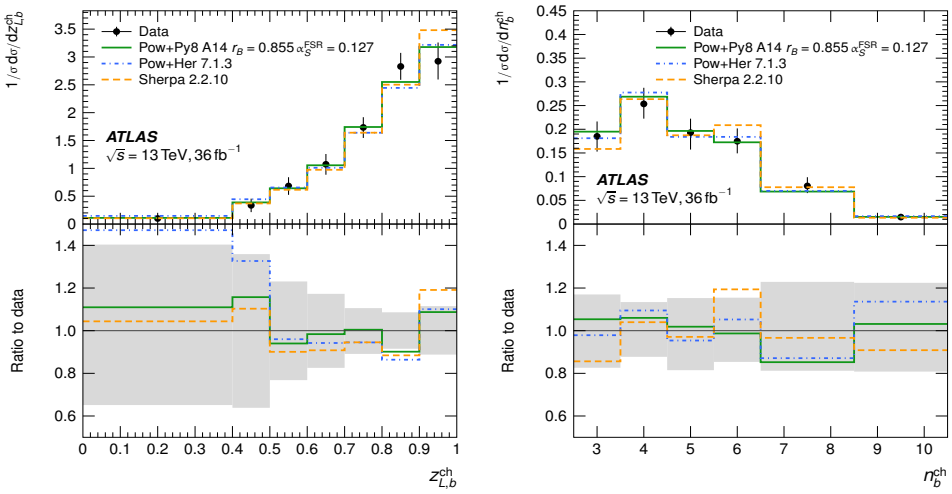

Figure 5. Distribution of the charged longitudinal profile of B hadrons inside jets (left). Distribution of the number of charged particles originating from the decay of the B hadron (right).

5 Summary and conclusions

Results by the ATLAS Collaboration, sensitive to various aspects of the modelling of QCD, have been presented. The measurements include variables sensitive to the initial state, which are used for determining the Parton Distribution Functions, as well as to the hard-scattering process. This includes the production cross section of Z bosons in association with high-p_T jets as well as the production cross section of photon pairs.

The strong coupling constant α_s is determined from fits to the Transverse Energy-Energy Correlation distributions in different kinematic ranges. The running of $\alpha_s(Q)$ is obtained and compared to previous measurements and to the prediction from the Renormalisation Group Equation.

The fragmentation of heavy quarks has been probed in two different analyses. The first of them presents a measurement of the longitudinal and transverse profiles of the momentum of charged B mesons, decaying via $B^{\pm} \to J/\psi K^{\pm}$, with respect to the jet containing them. The second one presents different distributions sensitive to the fragmentation of b-quarks obtained in dileptonic $t\bar{t}$ events.

References

[1] J.C. Collins, D.E. Soper and G. Sterman, [Nucl. Phys. B. 261, 104 (1985)].
[2] ATLAS Collaboration, [Eur. Phys. J. C 82, 438 (2022)].
[3] H1 and ZEUS Collaborations, [Eur. Phys. J. C 75, 580 (2015)].
[4] T-J. Hou *et al.*, [Phys. Rev. D 103, 014013 (2021)].
[5] R.D. Ball *et al.*, [Eur. Phys. J. C 77, 663 (2017)].
[6] S. Bailey *et al.*, [Eur. Phys. J. C 81, 341 (2021)].
[7] ATLAS Collaboration, [arXiv:2205.02597 (hep-ex)].
[8] J. Alwall *et al.* [JHEP 07, 079 (2014)].
[9] E. Bothmann *et al.* [SciPost Phys. 7, 034 (2019)]
[10] ATLAS Collaboration [arXiv:2112.09588 (hep-ex)].
[11] ATLAS Collaboration, [ATLAS-CONF-2020-025].
[12] ATLAS Collaboration, [JHEP 11, 169 (2021)].
[13] T. Binoth, J. P. Guillet, E. Pilon and M. Werlen, [Eur. Phys. J. C 16, 311 (2000)].
[14] ATLAS Collaboration [JHEP 12, 131 (2021)].
[15] ATLAS Collaboration [Phys. Rev. D 106, 032008 (2022)].